Journal of Information and Intelligence 1 (2023) 267–280

Contents lists available at ScienceDirect

Journal of Information and Intelligence

journal homepage: www.journals.elsevier.com/journal-of-information-and-intelligence

Rate optimization using low complex methods with reconfigurable intelligent surfaces

Saber Hassouna, Muhammad Ali Jamshed, Masood Ur Rehman, Muhammad Ali Imran, Qammer H. Abbasi *

James Watt School of Engineering, University of Glasgow, Glasgow G12 8QE, UK

ARTICLE INFO

Keywords:
Reconfigurable intelligent surfaces (RISs)
Orthogonal frequency division multiplexing (OFDM)
Data rate maximization
Semidefinite relaxation (SDR)
Strongest tap maximization (SDM)
Power method

ABSTRACT

With the help of a developing technology called reconfigurable intelligent surfaces (RISs), it is possible to modify the propagation environment and boost the data rates of wireless communication networks. In this article, we optimized the phases of the RIS elements and performed a fair power allocation for each subcarrier over the full bandwidth in a single-input-single-output (SISO) wideband system where the user and the access point (AP) are provided with a single antenna. The data rate or its equivalent channel power is maximized by proposing different low-complex algorithms. The strongest tap maximization (STM) and power methods are compared with the semidefinite relaxation (SDR) method in terms of computational complexity and data rate performance. Runtime and complexity analysis of the suggested methods are computed and compared to reveal the actual time consumption and the required number of operations for each method. Simulation results show that with an optimized RIS, the sum rate is 2.5 times higher than with an unconfigured surface, demonstrating the RIS's tremendous advantages even in complex configurations. The data rate performance of the SDR method is higher than the power method and less than the STM method but with higher computational complexity, more than 6 million complex operations, and 50 min of runtime calculations compared with the other STM and power optimization methods.

1. Introduction

The need for faster data rates has grown significantly and exponentially over the past few years. The proliferation of mobile phones and the emergence of services that demand high data rates (such online gaming and video streaming) are the key factors that are continually driving up this demand. Massive multiple-input-multiple-output (MIMO) and millimetre wave (mmWave) are enabling technologies for future communication systems. These technologies can provide wide bandwidths combined with improved beamforming and spatial-multiplexing benefits from the antenna arrays to satisfy the requirements for increased data rates and accommodate an increasing range of wireless equipments [1]. Despite having potentially large possible rate improvements, these technologies typically have higher hardware and power costs, necessitating a separate evaluation of the overall benefits of their application for each user scenario. In addition, they are unable to directly control the propagation channel, whose randomness nature can occasionally limit the effectiveness of these solutions.

* Corresponding author.
E-mail addresses: s.hassouna.1@research.gla.ac.uk (S. Hassouna), muhammadali.jamshed@glasgow.ac.uk (M.A. Jamshed), masood.urrehman@glasgow.ac.uk (M. Ur Rehman), muhammad.imran@glasgow.ac.uk (M.A. Imran), qammer.abbasi@glasgow.ac.uk (Q.H. Abbasi).

https://doi.org/10.1016/j.jiixd.2023.06.004
Received 23 January 2023; Received in revised form 2 May 2023; Accepted 12 June 2023
Available online 11 July 2023

The use of RIS is a recent method that enhances the quality of wireless channels [2–4]. It enables the receiver to concentrate the signal due to the combined impact of reflections from all RIS elements and the direct line-of-sight route between the transmitter and the receiver. This combination produces a focused beam in a specific direction [5]. Unlike wireless repeaters and relays, RISs have unique features such as configurability, no signal amplification requirements, and no need for complex processing, coding, and decoding techniques [6].

1.1. Related work

The sum rate in RIS-enhanced multi-user MISO downlink communications was maximized by the authors in Ref. [7]. The power allocation and the RIS reflection matrix were optimized alternatively using the majorization-minimization method by using the zero-forcing precoding at the BS. The authors in Ref. [8] also looked at the issue of weighted sum rate maximization. Three iterative techniques were developed for optimising the reflection coefficients in terms of various kinds of RIS reflection components within the alternating optimization (AO) framework in order to produce the transmit beamforming. In Ref. [9], the authors first provide a workable transmission protocol for estimating the channels in a MIMO-OFDM system via pilot training, and they then suggest an AO algorithm for optimising the RIS phase shifts and power allocation matrix. The authors in Ref. [10] discuss the sum data increase with the presence of mutual coupling in a SISO OFDM system and provide a simple method for channel estimation and RIS construction that includes realistic reflection amplitudes and binary RIS phase shifts. In order to increase the attainable average sum rate in a RIS-enhanced multi-user system, Ref. [11] presented a two-timescale transmission protocol as opposed to optimising the passive beamforming using the instantaneous CSI. In Ref. [12], the authors used the AO approach to increase the achievable data rate of a multi-stream MIMO communication system supported by RIS. Despite being a straightforward optimization technique to use, it may take several iterations to converge.

The literature has suggested a number of alternative optimization techniques for increasing the data rates in RIS-assisted wireless communication systems, which aims to identify a nearly ideal solution with tolerable computational complexity and run time. Heuristic solutions, such as semidefinite relaxations (SDR) [13–20], strongest signal path maximization in time domain [3,21] and successive convex approximations [9] are investigated by many authors in the literature. Applying the SDR and the successive convex approximation approaches require efficient optimization tools. Furthermore, the SDR needs Gaussian randomization methods to obtain the rank-one suboptimal solution. Considerable effort has been devoted to developing sophisticated algorithms that can identify high-quality solutions that are close to optimal. However, the computational complexity associated with these algorithms is often quite high, making them prohibitively expensive in practical settings where a large number of RIS elements are present. It is precisely in such situations that RIS is most valuable [22–24].

1.2. Contribution and organization of the paper

The contributions of this research are highlighted as follows.

- We maximize the data rate of the single-input-single-output (SISO) wideband system equipped with RIS surface and single antenna for both access point (AP) and user equipment. We formulate a joint optimization problem of the subcarriers power allocations and the phase shifts of the RIS elements. Then, we proposed an iterative power method to solve the non-convex problem resulting from the unit-modular constraint on each RIS element. It is noted that for large surfaces the reflection coefficients can be estimated by the column of the discrete Fourier transform (DFT) matrix [25]. We used the DFT beamforming codebook to select an signal-to-noise ratio (SNR) maximizing configuration to be utilized in the proposed power method.
- To evaluate the performance of the power method in terms of the data rate and complexity computation, it is compared with the SDR method. The SDR approach handles the nonconvexunit-modulus constraint by transforming the passive beamforming vector into a rank-one and positive semidefinite matrix. The non-convex problem is transformed into a convex semidefinite program (SDP) problem by utilizing the SDR technique, which may then be addressed by a variety of effective convex optimization tools. The SDR method shows a higher performance data rate than the power method but at the cost of increased computational complexity and runtime. However, it shows lower performance than the strongest tap maximization (STM) method. The STM chooses a configuration that is good for channel tap rather than a subcarrier, when there exits a stronger a line-of-sight (LoS) path.
- The goal of this article is to demonstrate that the heuristic approaches like power and STM methods show significantly less computational complexity than the famous SDR method and achieve comparable data rates as a state-of-the-art benchmark scheme. The performance of all the methods is validated by comparing them with the upper bound of the system.

The rest of the paper is organized as follows. Section 2 presents the system and channel models. In Section 3, the data rate optimization using different methods is studied. A problem formulation is presented and followed by proposing a solution using different optimization methods. We computed the complexity and runtime for each method at the end of this section. The simulation results are discussed in Section 4 while the conclusion is given in Section 5.

2. System model

A single antenna (transmitter) and a single user (receiver) are used in a SISO wideband system. As depicted in Fig. 1, a RIS with N reconfigurable elements is taken into consideration inside the coverage area of the transmitter and receiver. An orthogonal frequency

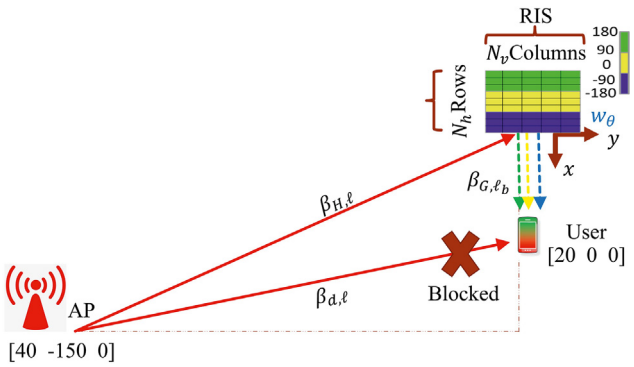

Fig. 1. System setup illustration.

division multiplexing (OFDM) is used for transmission. In the complex baseband domain, if $s(k)$ is the transmitted discrete-time signal, then the discrete-time received signal at the receiver can be written as [3]:

$$y[k] = \sum_{l=0}^{M-1} h_\theta[l]s[k-l] + e[k], \tag{1}$$

where, the wideband channel in the time-domain with the RIS configuration θ is represented as $\{h_\theta[l] : l = 0, \cdots, M-1\}$ and $e[k] \sim \mathcal{N}_{\mathbb{C}}(0, \sigma^2)$ is the receiver noise. The $h_\theta[l]$ is given by:

$$h_\theta[l] = h_d[l] + u_l^T w_\theta, \tag{2}$$

where, $h_d[l]$ and $u_l \in \mathbb{C}^N$ are the AP-User uncontrollable direct channel and the AP-RIS-User controllable indirect channels via all RIS N elements respectively. The reflection coefficients of all elements is described by $w_\theta \in \mathbb{C}^N$. With $K > M$ subcarriers and a length of $M-1$ cyclic prefix, an OFDM transmission is taken into consideration. As a result, a time domain signal with a block of $K + M - 1$ is transmitted to generate a block of OFDM signal with K of parallel subcarriers by using the DFT:

$$\bar{y}[\nu] = \bar{h}_\theta[\nu]\bar{s}[\nu] + \bar{e}[\nu], \quad \nu = 0, \cdots, K-1. \tag{3}$$

The above equation (3) can be illustrated in vector form as follows:

$$\begin{bmatrix} \bar{y}[0] \\ \vdots \\ \bar{y}[K-1] \end{bmatrix} = \begin{bmatrix} \bar{h}_\theta[0] \\ \vdots \\ \bar{h}_\theta[K-1] \end{bmatrix} \odot \begin{bmatrix} \bar{s}[0] \\ \vdots \\ \bar{s}[K-1] \end{bmatrix} + \begin{bmatrix} \bar{e}[0] \\ \vdots \\ \bar{e}[K-1] \end{bmatrix}, \tag{4}$$

where, $\odot$ describes the hadamard product. The channel vector $\bar{h}_\theta$ can be realized a function of w_θ as per following:

$$\bar{h}_\theta = F \begin{bmatrix} h_d[0] + u_0^T w_\theta \\ \vdots \\ h_d[M-1] + u_{M-1}^T w_\theta \end{bmatrix} = F(h_d + U^T w_\theta), \tag{5}$$

where, $h_d = [h_d[0], \cdots, h_d[M-1]]^T$ and $U = [u_0, \cdots, u_{M-1}] \in \mathbb{C}^{N \times M}$ are the AP-User uncontrollable direct channel components and the AP-RIS-User controllable indirect propagation channels respectively. The channel parameters will be defined later, in the channel model. We assume that the channel models are known in the system. The (ν, k)th element of the DFT matrix $F \in \mathbb{C}^{K \times M}$ is $e^{-\frac{2\pi k\nu}{K}}$. The reflection coefficients of the RIS that accounts for the effective phase shifts $(\theta_1, \theta_2, \cdots, \theta_N) \in [-\pi, \pi)$ and amplitude coefficients $(\gamma_1, \gamma_2, \cdots, \gamma_N) \in [0, 1]$ are included in the vector $w_\theta = [w_{\theta_1}, \cdots, w_{\theta_N}]^T \in \mathbb{C}^{N \times 1}$. The sum data transmission rate across K subcarriers, given a specific RIS setup, assuming uniform power distribution and known channel at the receiving end, is expressed as:

$$R = \frac{B}{K+M-1} \sum_{\nu=0}^{K-1} \log_2 \left(1 + \frac{P_\nu \left| f_\nu^H h_d + f_\nu^H U^T w_\theta \right|^2}{BN_o} \right) \frac{bit}{s}, \tag{6}$$

the channel bandwidth represented by B, the power allocated to the subcarrier ν indicated by P_ν, the number of channel taps referred to as M, and the f_ν^H component, which corresponds to the νth row of DFT matrix F. It is worth noting that the upper bound of equation (6) is provided in Ref. [3]:

$$R \leq \frac{B}{K+M-1}\sum_{v=0}^{K-1}\log_2\left(1+\frac{P_v}{BN_o}\left(\left|f_v^H h_d\right|+\ \|\, f_v^H U^T\ \|_1\right)^2\right), \tag{7}$$

where, $\|\cdot\|_1$ is the L_1 norm.

2.1. Channel model

The uncontrollable direct channel is given by Ref. [10]:

$$h_d = \sum_{\ell=1}^{L_d}\left(\beta_{d,\ell}\right)^{\frac{1}{2}} e^{-j2\pi f_c \tau_{d,\ell}}\begin{bmatrix}\operatorname{sinc}(0+B(\alpha-\tau_{d,\ell}))\\ \vdots \\ \operatorname{sinc}(M-1+B(\alpha-\tau_{d,\ell}))\end{bmatrix}, \tag{8}$$

where, $\beta_{d,\ell}$ is the ℓ^{th} pathloss from the AP to the user with L_d propagation paths as per Fig. 1, $\tau_{d,\ell}$ is the delay of propagation and the sampling delay over the shortest path is α. Similarly, the controllable indirect channel is presented as:

$$U = \sum_{\ell=1}^{L_a}\sum_{\ell_b=1}^{L_b}\left(\beta_{H,\ell}\beta_{G,\ell_b}\right)^{\frac{1}{2}} e^{-j2\pi f_c\left(\tau_{H,\ell}+\tau_{G,\ell_b}\right)}\left(a\left(\phi_{H,\ell},\vartheta_{H,\ell}\right)\odot a\left(\phi_{G,\ell},\vartheta_{G,\ell_b}\right)\right)\begin{bmatrix}\operatorname{sinc}(0+B(\alpha-\tau_{H,\ell}-\tau_{G,\ell}))\\ \vdots \\ \operatorname{sinc}(M-1+B(\alpha-\tau_{H,\ell}-\tau_{G,\ell_b}))\end{bmatrix}^T, \tag{9}$$

the paths L_a and L_b represent the propagation of signals from the AP to the RIS, and from the RIS to the users, respectively. The attenuation of the combined indirect channel from the AP to the user via the RIS is denoted by $\beta_{H,\ell} \geq 0$, and $\beta_{G,\ell_b} \geq 0$, as depicted in Fig. 1. The time delay for propagation along the paths to and from the RIS is $\tau_{H,\ell}$ and τ_{G,ℓ_b}, respectively. The array response vector is denoted by $a(\varphi,\vartheta) = \sqrt{\mathcal{G}(\varphi,\vartheta)}\left[e^{j\mathcal{K}(\varphi,\vartheta)^T\mathbb{U}_1},\cdots,e^{j\mathcal{K}(\varphi,\vartheta)^T\mathbb{U}_N}\right]^T$, where $\mathcal{G}(\varphi,\vartheta)$ represents the directivity pattern of each element, and ϑ and ϕ denote the elevation and azimuth angles, respectively. The wavenumber, $\mathcal{K}(\varphi,\vartheta) = \frac{2\pi}{\lambda}[\cos\vartheta\cos\varphi,\cos\vartheta\sin\varphi,\sin\vartheta]^T$, is also included in the equation. The location of the mth element is represented by $\mathbb{U}_m = [0,i(m)0.25\lambda,j(m)0.25\lambda]^T$, where $i(m) = \mod(m-1,N_h)$ and $j(m) = \lfloor(m-1)/N_h\rfloor$ correspond to the horizontal and vertical indices of element m. The modulus and truncate operations are represented by $\mathrm{mod}(\cdot,\cdot)$ and $\lfloor\cdot\rfloor$, respectively. Finally, the vertical and horizontal spacing between the elements is $\lambda/4$, where $\lambda = 0.075$ m.

3. The data rate optimization using different methods

A more challenging RIS optimization problem arises in the wideband scenario with K orthogonal subcarriers than in the narrowband case with a single subcarrier. Estimating the ideal vector w_θ and fairly assigning the power to each subcarrier are necessary for maximizing the data rate in equation (6). In a one-bit RIS architecture, each RIS element can alternate between the phase shifts of 90° or −90°. The phase matrices can be created from the DFT columns of the beamforming codebook [25].

3.1. Beamforming 2D-DFT codebook

Finding the optimal configuration involves a lengthy analysis and is essentially impossible for large values of N because there are 2^N possible RIS configurations. In existing research, switching between N orthogonal configurations for a RIS with N reflecting elements depends on accurate configurations. The structure of the optimal RIS phase shifts remains compatible with the 2D-DFT codebook for a given incident and desired reflected angles [25]. Therefore, if an incoming signal is directed towards a particular beam, each column of the codebook beamformer $W_\theta = F(N_v)\otimes F(N_h) \in \mathbb{C}^{N\times N}$, (where $\otimes$ represents the Kronecker product) may correspond to a potential reflection configuration. As a result, for this codebook setup, the likelihood of obtaining a strong SNR configuration is significantly high. The DFT matrices for the columns $F(N_v)$ and $F(N_h)$ can be denoted as:

$$F(N_v) = \begin{bmatrix}1 & 1 & 1 & \cdots & 1\\ 1 & f_{N_v} & f_{N_v}^2 & \cdots & f_{N_v}^{N_v-1}\\ \vdots & \vdots & \vdots & & \vdots\\ 1 & f_{N_v}^{N_v-1} & f_{N_v}^{2(N_v-1)} & \cdots & f_{N_v}^{(N_v-1)(N_v-1)}\end{bmatrix}, \tag{10}$$

in this context, $f_{N_v} = e^{-j2\pi/N_v} = \cos(2\pi/N_v) - \sin(2\pi/N_v))$. The variables N_v and N_h correspond to the number of vertical and horizontal elements, respectively, within the RIS, as shown in Fig. 1. To fit the RIS design, the phase shifts produced by the codebook should be quantized. Therefore, the reflection coefficient w_θ for element i can be either $e^{j\pi/2}$ if $\arg\left([w_\theta]_i\right) \in [-\pi,0)$ or $e^{-j\pi/2}$ if $\arg\left([w_\theta]_i\right) \in [0,\pi)$. We looked through the codebook W_θ to find the best configuration that will maximize the SNR in equation (11). The best phase configuration that can be created from the codebook can be represented as $w_{\theta_{\text{CodeBook}}} \in W_\theta$. It is considered the standard or reference point for achieving the maximum SNR:

$$SNR = \frac{P|\bar{h}_\theta|^2}{BN_o}. \tag{11}$$

Algorithm 1 utilizes the optimal configuration with the highest SNR, which is determined by evaluating P across all numbers of subcarriers.

Algorithm 1: Proposed power method for optimizing $\|\bar{h}_\theta\|^2$.

1: Input: $w_{\theta_{\text{CodeBook}}}$, Ω_0, $h_{\text{equivalent}}$.
2: Output: $w_{\theta_{\text{optimized}}}$.
3: Select $w_{\theta_{\text{CodeBook}}}$ from the codebook $\{W_\theta\}$ that gives the maximum SNR in equation (11) and set $w_\theta = w_{\theta_{\text{CodeBook}}}$ so, $\Omega_0 = \begin{bmatrix} 1 \\ w_\theta \end{bmatrix}$.
4: Set $n = 1$
5: **for** $n <$ maximum number of iterations **do**
6: Compute $\mathcal{H}_i = h_{\text{equivalent}}\,\Omega_i$ from the initial solution Ω_0 and let the first entry $H_{i,1} = \text{sign}(\mathcal{H}^*_{i,1}\mathcal{H}_{i,1})$ to ensure that the direct path is always assigned to 1 and unconnected with the RIS configurations. sign(·) is the signum function.
7: Set $\Omega_{i+1} = \mathcal{H}_i$ and then quantize the current phases of all candidates $([w_\theta]_i)$ where $i = 1, \cdots, N$ to be either $\{e^{j\pi/2}$ or $e^{-j\pi/2}\}$ if $\arg([w_\theta]_i) \in [-\pi, 0)$ and $\arg([w_\theta]_i) \in [0, \pi)$ respectively.
8: Iterate until convergence
9: **end for**
10: After convergence $w_{\theta_{\text{optimized}}}$ is obtained.
11: Calculate the power allocation for subcarriers P_v as per equation (25).
12: Evaluate the data rate R in equation (6) by substituting $w_\theta = w_{\theta_{\text{optimized}}}$ and the optimized P_v resulting from equation (25).

3.2. Problem formulation

The objective of this research is to enhance the sum rate received by the user by optimising the transmit power P and reflection coefficient vector w_θ across all the RIS elements. The optimization problem (OP1) can be formulated mathematically to represent the problem of maximizing the sum rate:

$$\begin{cases} (\text{OP1}): \max\limits_{P, w_\theta} R(P, w_\theta) = \sum\limits_{v=0}^{K-1} \log_2\left(1 + \dfrac{P_v |f_v^H h_d + f_v^H U^T w_\theta|^2}{BN_o}\right), \\ \text{s.t.} \quad (C1): |[w_\theta]_i| = 1, \ \forall i \in N, \ (C2): \dfrac{1}{K}\sum\limits_{v=0}^{K-1} P_v \le P, \ (C3): P_v \ge 0, \ \forall_v \in K. \end{cases} \tag{12}$$

The first constraint (C1) confirms that there is no pathloss in the reflection of each RIS element. It is necessary to use unit magnitude elements as RIS elements do not amplify or decode signals like relays. Constraint (C2) specifies that power allocations across all subcarriers must not exceed the power budget of the base station and should be ≥ 0, as indicated in constraint (C3). It is important to note that the non-convexity of the (OP1) over the unit modular constraint (C1) for all RIS elements [9] is addressed by iteratively utilizing the power method until convergence is achieved, leading to the optimal w_θ that can impact all subcarriers. Furthermore, the power in constraint (C2) is allocated to each subcarrier using the well-established water-filling algorithm.

3.3. Proposed solutions

3.3.1. Power method

In order to optimize the RIS phase shifts, we employ the power method to identify a low-complex solution. It determines the channel power's dominating eigenvector. The channel power is given as follows:

$$\|\bar{h}_\theta\|^2 = \underbrace{\begin{bmatrix} 1 \\ w_\theta \end{bmatrix}^H}_{\Omega^H} \underbrace{[h_d, U^T]^H [h_d, U^T]}_{h_{\text{equivalent}}} \underbrace{\begin{bmatrix} 1 \\ w_\theta \end{bmatrix}}_{\Omega}. \tag{13}$$

We consider that the channels h_d and U are known at the receiver. To initiate the power method and optimize the quadratic form of the channel $\|\bar{h}_\theta\|^2$, we select $w_{\theta_{CodeBook}}$ from the codebook $W_\theta \in \mathbb{C}^{N \times N}$ as shown in Algorithm 1. The power method determines the dominant eigenvalue by iteratively computing $\Omega_{i+1} = \frac{h_{\text{equivalent}}\,\Omega_i}{\|h_{\text{equivalent}}\,\Omega_i\|}$ from the initial solution $\Omega_0 = \begin{bmatrix} 1 \\ w_\theta \end{bmatrix}$, where we set $w_\theta = w_{\theta_{\text{CodeBook}}}$, until convergence, following the steps outlined in Algorithm 1.

3.3.2. Semidefinite relaxation method

The vth ($v = 0, 1, \cdots, K-1$) subcarrier has a channel gain as follows:

$$\|\bar{h}_\theta\|^2 = \sum_{v=0}^{K-1} \left| f_v^H h_d + f_v^H U^T w_\theta \right|^2. \tag{14}$$

The channel gain fluctuates as a function of the passive beamforming vector w_θ. In order to increase the data rate in equation (6), we develop an optimization problem, relying on equation (14), using beamforming reflection coefficient vector w_θ and fairly allocating the power over the entire subcarriers. The optimization problem below is specifically reformulated as follows:

$$\begin{cases} \text{(OP2)}: \max\limits_{P, w_\theta} \sum\limits_{v=0}^{K-1} \left| f_v^H h_d + f_v^H U^T w_\theta \right|^2, \\ \text{s.t. (C1)}: \ \left| [w_\theta]_i \right| = 1, \quad \forall i \in N, \quad \text{(C2)}: \ \dfrac{1}{K} \sum\limits_{v=0}^{K-1} P_v \le P, \quad \text{(C3)}: \ P_v \ge 0, \quad \forall_v \in K, \end{cases} \tag{15}$$

where unnecessary terms have been removed for the sake of clarity. Keep in mind that the sum channel gain maximization at the user is the optimal value of (OP2). Through the use of the semidefinite relaxation approach, we are able to solve the problem (OP2) sub-optimally. Thus, the (OP2) objective function of equation (15) is denoted as:

$$\widetilde{U} = \sum_{v=0}^{K-1} f_v^H U U^H, \tag{16}$$

$$\widetilde{u} = \sum_{v=0}^{K-1} f_v^H U h_d, \tag{17}$$

$$\widetilde{D} = \sum_{v=0}^{K-1} \left| f_v^H h_d \right|^2, \tag{18}$$

where (OP2) is equivalent to:

$$\begin{cases} \text{(OP3)}: \max\limits_{w_\theta} w_\theta^H \widetilde{U} w_\theta + w_\theta^H \widetilde{u} + \widetilde{u}^H w_\theta + \widetilde{D}, \\ \text{s.t.} \ \left| [w_\theta]_i \right| = 1, \forall i = 1, 2, \cdots, K, \ \dfrac{1}{K} \sum\limits_{v=0}^{K-1} P_v \le P, P_v \ge 0, \forall_v \in K. \end{cases} \tag{19}$$

Problem (OP3) is easily distinguishable as a non-convex quadratically constrained quadratic programme (QCQP) problem, which can be rewritten as a homogeneous QCQP problem. In particular, by describing:

$$Q = \begin{bmatrix} \widetilde{U} & \widetilde{u} \\ \widetilde{u}^H & 0 \end{bmatrix}, \widetilde{w}_\theta = \begin{bmatrix} w_\theta \\ t \end{bmatrix}, \tag{20}$$

where, t is an auxiliary variable. Let us define $\phi = \widetilde{w}_\theta \widetilde{w}_\theta^T$ with rank $(\phi) = 1$. Optimization Problem (OP3) is changed into the following problem:

$$\begin{cases} \text{(OP4)}: \max\limits_{\phi} \operatorname{tr}(Q\phi) + \widetilde{D}, \\ \text{s.t.} \ [\phi]_{i,i} = 1, \forall i = 1, 2, \cdots, N+1, \phi \ge 0. \end{cases} \tag{21}$$

It is noted that due to the rank-one constraint, (OP4) is still not convex. As a result, We apply the SDR method to overcome the rank-one constraint, transforming (OP4) into a convex SDP that can be solved effectively with the help of current convex optimization solvers like CVX [26]. It is important to note that the ideal objective value of (OP4) acts as an upper bound on that of (OP2). However, the best solution ϕ^* to (OP4) might not be a rank-one answer. As a consequence, using the Gaussian randomization method, we produce the following rank-one solution:

$$\phi^* = \Lambda \Sigma \Lambda^H, \tag{22}$$

where $\Lambda = [\rho_1, \cdots, \rho_{N+1}]$ and $\Sigma = \operatorname{diag}(\boldsymbol{\alpha}_1, \cdots, \boldsymbol{\alpha}_{N+1})$ are unitary and diagonal matrices, respectively, both with the size of $(N+1) \times (N+1)$. Then we obtain a suboptimal solution to (OP4) as $\widetilde{w}_\theta^* = \Lambda \Sigma r$ where $r \in \mathbb{C}^{(N+1)\times 1}$ is a random vector generated according to $r \in \mathcal{N}_{\mathbb{C}}(0, I_{N+1})$ denoting the circularly symmetric complex Gaussian (CSCG) distribution with zero mean and covariance matrix I_{N+1}. Finally, we achieve a suboptimal solution to the issue (OP2) as $w_\theta{}^* = e^{j\angle([\widetilde{w}_\theta{}^*]_{1:N} / [\widetilde{w}_\theta]_{N+1})}$.

3.3.3. Strongest tap maximization method

According to STM, the received signal power should be concentrated in the time domain rather than distributed over the K subcarriers. Therefore, choosing a configuration that is suitable for a single channel tap is preferable to the one which is suitable for a single subcarrier. This is especially valid if one of the LoS propagation paths is significantly more powerful than all other paths. It should be noted that the total energy of the incoming signals, computed in the frequency domain, is the objective function in equation (15). The optimization problem (OP2) is thus equivalent to the following problem:

$$\begin{cases} (\text{OP5}): \max\limits_{w_\theta} \sum\limits_{l=0}^{M-1} h_d[l] + v_l^T w_\theta, \\ \text{s.t.} \ \left|[w_\theta]_i\right| = 1, \forall_i \in N. \end{cases} \tag{23}$$

Because practical wireless communication systems have $M \ll K$, it should be noted that computing the objective function in equation (23) is more effective than calculating it in equation (15). To start, we determine the vector w_θ that increases the magnitude of every channel tap. We then select the solution resulting in the largest magnitude with respect to the channel tap index l:

$$\ell^{\text{opt}} = \underset{\ell \in \{0,\cdots,M-1\}}{\arg\max} \left| h_d[\ell] + u_\ell^{\text{T}} \omega_\ell \right|^2. \tag{24}$$

Consequently, we obtain the following sub-optimal solution to the problem (OP2) as $w_{\theta_l} = \left[e^{\mathrm{j}\left(\arg(h_d[l]) - \arg\left([u_l]_1\right)\right)}, \cdots, e^{\mathrm{j}\left(\arg(h_d[l]) - \arg\left([u_l]_N\right)\right)} \right]^{\text{T}}$, where the argument of a complex number is provided by $\arg(\cdot)$ and the nth entry of u_l is signified by $[u_\ell]_n$. The phase of every component in the inner product $u_l^{\text{T}}\omega_l$ is rotated in this solution to line up with the phase of $h_d[\ell]$.

3.3.4. Water-filling algorithm

All subcarriers $P_0, \cdots, P_{K-1}$ have a power distribution that satisfies $P = \frac{1}{K}\sum_{v=0}^{K-1} P_v$, where $P_v = E\left\{|\bar{s}[v]|^2\right\}$ is the power assigned to subcarrier v. The symbol $E\{\cdot\}$ represents the expectation operator. To determine the optimal amount of power assigned to each subcarrier, the water-filling algorithm [9] can be employed:

$$P_v = \max\left(\eta - \frac{BN_o}{\left|f_v^H h_d + f_v^H U^T w_\theta\right|^2}, 0\right), \tag{25}$$

where, the parameter $\eta \geq 0$ is chosen to satisfy $\frac{1}{K}\sum_{v=0}^{K-1} P_v = P$. Consequently, the power allocated for vth subcarrier P_v is dependent on the water level parameter η and can be re-written as follows:

$$P_v = \begin{cases} \eta - \dfrac{BN_o}{\left|f_v^H h_d + f_v^H U^T w_\theta\right|^2}, & \text{if } \eta \geq \dfrac{BN_o}{\left|f_v^H h_d + f_v^H U^T w_\theta\right|^2} \\ 0, & \text{if } \eta < \dfrac{BN_o}{\left|f_v^H h_d + f_v^H U^T w_\theta\right|^2} \end{cases}. \tag{26}$$

The water-filling algorithm is used to allocate the transmitted power fairly to all subcarriers in the different optimization methods, STM, SDR, power method and the case when the surface is unconfigured. In Fig. 2, we show how the water-filling algorithm allocates the 15 watt power for the entire number of subcarriers fairly taking into consideration the channel gain status. The black circles in the figure refer to the amount of power allocated by the algorithm to some subcarriers taking into consideration their corresponding noise to signal ratio status.

3.4. Computational complexity

This section discusses the computational complexity of the proposed optimization methods for allocating fair power to all subcarriers and tuning phases of the RIS. To estimate the Big-O ($\mathcal{O}$) complexity of these methods, we followed the same procedure as in Ref. [1]. The complexity of the power method can be calculated by considering the steps in Algorithm 1. The algorithm requires $(N+1)^2$ complex multiplications for the term $h_{\text{equivalent}}$, while the term $h_{\text{equivalent}}\,\Omega_i$ necessitates $(N+1)$ complex multiplications and phases quantization demands N complex computations. Additionally, allocating power to all subcarriers requires $2(KM)$ complex multiplications. Thus, the estimated overall complexity per iteration is denoted as $\mathcal{O}_{\text{Power}}$:

$$\mathcal{O}_{\text{Power}} = \mathcal{O}\left(\left((N+1)^2 + (N+1) + N\right)I_R + 2(KM)\right), \tag{27}$$

where, I_R represents the maximum number of iterations required to achieve the optimal data rate. The complexity of the SDR method can be determined by calculating the complex operations of the following terms. The terms Q and ϕ in equation (20) require $(N+1)^2$ complex multiplications for each of them. The Gaussian randomization method needs $(N+1)^{4.5}$ complex multiplications to compute the best solution ϕ^*. Moreover, power allocation for all subcarriers, as per Fig. 2 SDR method, needs $2(KM)$ complex multiplications. Consequently, the overall estimated complexity is given as $\mathcal{O}_{SDR}$:

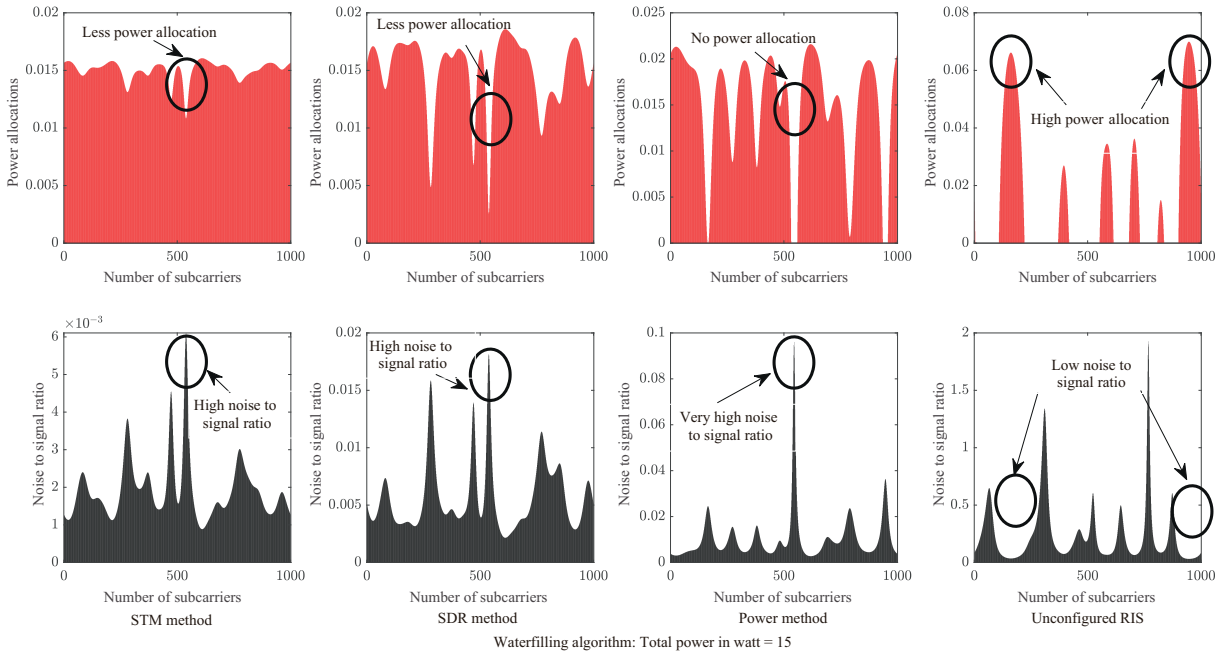

Fig. 2. Fair Power allocations for all subcarriers in STM method, SDR method, Power method and the case when the RIS surface is unconfigured.

$$\mathscr{O}_{SDR} = \Big(2(N+1)^2 + (N+1)^{4.5} + 2(KM)\Big). \tag{28}$$

The complexity in equation (28) meets with the computational complexities estimated in Refs. [9,13]. The complexity in Ref. [9] is $\mathscr{O}\left(NKI_{SA} + N^{4.5}K^{3.5}I_T\right)$ where I_{SA} denotes the number of iterations that the successive approximation requires and I_T is the total time that is needed to solve the problem during the successive convex approximation algorithm. Furthermore, the complexity is calculated as $\mathscr{O}(N+1)^{4.5}$ in Ref. [13]. Consequently, the complexity in equation (28) coincides with the results in Refs. [9,13] in terms of the complexity degree of $\mathscr{O}(N)^{4.5}$. Furthermore, the complexity for STM method is computed using the same procedure:

$$\mathscr{O}_{STM} = \mathscr{O}((N) + 2(KM)). \tag{29}$$

The methods complexities are compared in Table 1. It is obvious from Table 1 that the SDR complexity is the highest in terms of $\mathscr{O}(N)^{4.5}$ while the STM is the lowest in terms of $\mathscr{O}(N)$ and the power method is lying in between SDR and STM with Complexity $\mathscr{O}(N)^2$.

4. Simulation results

We analyze the performance of our suggested approaches for increasing the RIS-aided SISO-OFDM system achievable data rate by providing numerical results from Monte Carlo simulations. The simulation parameters are considered by using the 3GPP channel model [27] and Table 2. In this study, we take into account an OFDM system with number of subcarriers $K = 1000$ and a more realistic multi-path channel model with channel taps $M = 23$ at random delays and an exponential power decay profile. The AP, user, RIS locations coordinates in meter are shown in Fig. 1. We considered LoS channels between the AP-RIS-User indirect link as per Fig. 1, to guarantee effective transmissions and large channel gains. However, the NLoS propagation is assumed between the AP and the user direct link. We contrast the achieved data rate of the suggested methods with the system's upper bound. For Comparison with the system upper bound, we consider the power method, SDR, STM benchmark schemes and the case when the surface is Un-configured where we replaced the RIS with a passive metal sheet causing zero phase-shifts for the entire elements.

The data rate of the proposed methods is compared in Fig. 3 considering LoS channels between the AP-RIS-User indirect link as per Fig. 1. The heuristic STM method outperforms both the SDR and the power methods while the data rate is the lowest in case of the

Table 1
Proposed methods complexities and qualities.

Method	Complexity	Objective function	Quality
Power	$\mathscr{O}(((N+1)^2 + (N+1) + N)I_R + 2(KM))$	Equivalent power of the channel	Low complex and suboptimal solution
SDR	$\mathscr{O}(2(N+1)^2 + (N+1)^{4.5} + 2(KM))$	Equivalent power of the channel	High complex and suboptimal solution
STM	$\mathscr{O}((N) + 2(KM))$	Equivalent power of the channel	Low complex and suboptimal

unconfigured RIS (metal sheet). The achievable data rate is dramatically boosted up as the range of subcarriers increases. In comparison to unconfigured RIS (metal sheet) configuration, the proposed approaches improve the sum data rate dramatically with an optimized RIS because of the adjusted RIS coefficients that allow the direct and reflecting channels to be integrated at the receiver more effectively and constructively. The power method shows the lowest data rate among the other methods however, it is a practical way to configure the RIS surface by implementing the strongest SNR configuration selected from the W_θ codebook. The SDR method outperforms the power method by optimising the quadratic form of the channel power, however, the STM method shows the highest achievable data rate since it implements the dominant LoS in the composite AP-RIS-User channel.

Unlike the scenario in Figs. 3 and 4 incorporates the example when the path to the RIS encounters an NLoS, which sheds light on two influences: There is no dominant path, and the path via the RIS is weaker. The upper bound and the unconfigured RIS surface (metal sheet) are much closer together due to the weaker path through the RIS, whereas the absence of the dominating path leads to the impossibility to identify a single RIS configuration that works for the total number of subcarriers. Fig. 4 results meet with Ref. [3] when the authors demonstrated the same scenario for the STM method and the upper bound cases.

An important parameter that should be taken into account when investigating the data rate is the dimension of the RIS surface. The RIS enhances the data rate and it increases further when the surface is large are per Fig. 5. We compare the achievable rate of different schemes versus the number of RIS elements at SNR = 20 dB. It is clear that the rate performance of the un-configured surface (zero phase shifts) scheme at the RIS is independent of the number of elements. However, the tuned RIS phase profiles in the other schemes (STM, SDR and power method) enhanced the data rate with the increase number of RIS elements. The highest average data rate over the entire bandwidth is shown when the number of elements on the surface is $N = 400$, while the lower data rate is obtained at $N = 100$ or less.

Another crucial factor that should be considered is the complexity and runtime. Table 1 reveals the complexity level for each method. The complexity in SDR method is $\mathcal{O}(N^{4.5})$ while it is very less in both power and STM methods, $\mathcal{O}(N^2)$ and $\mathcal{O}(N)$ respectively. We illustrated the complexity level and the runtime consumption for each method in Figs. 6 and 7 respectively. We noticed that the SDR

Table 2
Simulation parameters.

Parameter	Value
Carrier frequency f_c	4e9 Hz
Speed of light C	3e8 m/s
Wavelength λ	0.075 m
Total number of elements N	400
Number of horizontal elements $N_h = 64$	20
Number of vertical elements $N_v = 64$	20
Vertical and horizontal element spacing	$\lambda/4$
AP location in meter, coordinates $[x, y, z]$	$[40\ \ -150\ \ 0]^T$
User location in meter, coordinates $[x, y, z]$	$[20\ \ 0\ \ 0]^T$
RIS location in meter, coordinates $[x, y, z]$	$[0\ \ 0\ \ 0]^T$
Pathloss NLoS	$34.53 + 38\log_{10}(d)$
Pathloss LoS	$30.18 + 26\log_{10}(d)$
Channel taps M	23
Total number of subcarriers K	1000
Transmitted power P	15 W
Bandwidth B	15e6 Hz

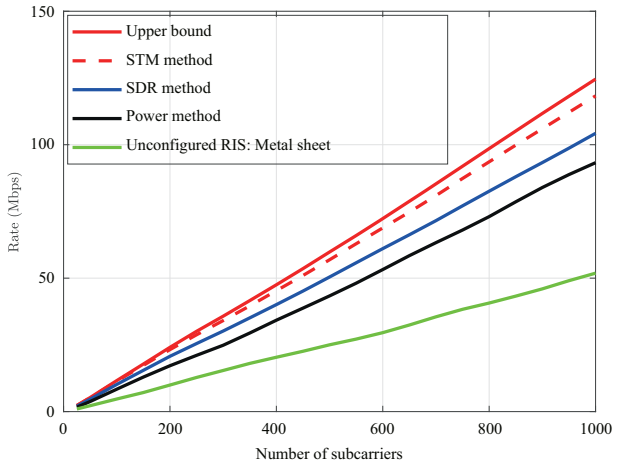

Fig. 3. Comparison of data rate versus the number of subcarriers when considering LoS channel between the AP-RIS-User composite indirect link.

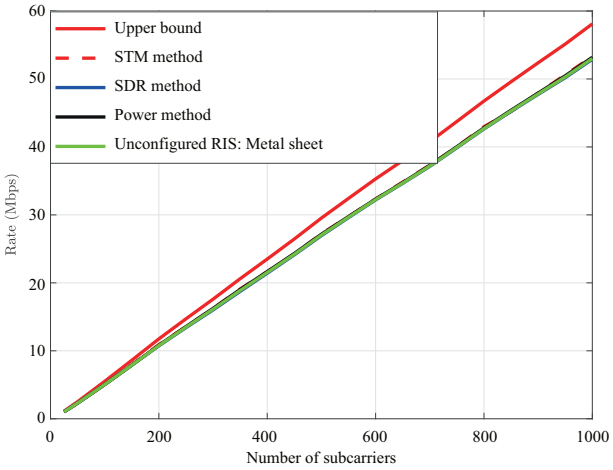

Fig. 4. Comparison of data rate versus the number of subcarriers when considering NLoS channel between the AP-RIS-User composite indirect link.

method complexity is the highest (more than 6 millions of complex multiplications) with a runtime larger than 50 min, however, the complexity in the other two methods, STM and the power method, is less than the SDR with few minutes runtime consumption.

The above simulation results considered low finite resolution phase shift configurations. Two phase configurations (1-bit RIS) $\theta_n \in \{0, \pi\}$ or $\{\frac{\pi}{2}, -\frac{\pi}{2}\}$ are used to maximize the SNR at the user. It is preferable, for more realistic and practical scenarios in the design, to select the phase shifts which are limited to a certain number of states. The higher resolutions necessitate complex RIS design with different bias voltages dedicated for each state. For example, in 2-bit RIS scenario four phase configurations are required for each RIS cell or element while the 3-bit RIS design switch over to eight-phase configurations. The channel gains $\beta_{H,\ell}$ and β_{G,ℓ_b} move along the unit circle with these phase shifts configurations while the path $\beta_{d,\ell}$ cannot be moved since it is the direct channel path as per Fig. 1. Consequently, if 1-bit RIS design is considered then one should select 0 or π phase shift. If 0 phase shift is selected, then the gains $\beta_{H,\ell}$ and β_{G,ℓ_b} will remain at the location where they are on the unit circle, however, if π is chosen then the gains will move to the opposite side of the circle. The key point is to shift theses signal gains $\beta_{H,\ell}$ and β_{G,ℓ_b} in the same half-space of the unit circle as the direct channel gain so, one can add all the terms $(\beta_{d,\ell}, \beta_{H,\ell}$ and $\beta_{G,\ell})$ constructively. The same procedure can be repeated for higher resolutions of phases where all the signals are added up in the same quadrant of the unit circle as the direct path. Therefore, higher phase resolutions are not required as long as the signals can be added constructively without cancelling each other. An illustration is shown on the unit circle for two and four finite phase resolutions when the RIS has two elements only for simplicity [3]. All the signals are gathered in the same half space in the two configurations case while they are in the same quadrant in the four configurations case as per Fig. 8.

The finite phase resolutions for different bit-RIS designs are studied in the case of the STM scheme. The obtained results of the sum data rate in case of higher-bit RIS are very close to the 1-bit and 2-bit RIS and this is expected since the path phases of the indirect channels are aligned with the dominant LoS path of the direct channel gain in the STM method. Consequently, they are added up constructively at the receiver and hence increase the SNR and the sum rate. However, choosing higher-bit RIS design increase the

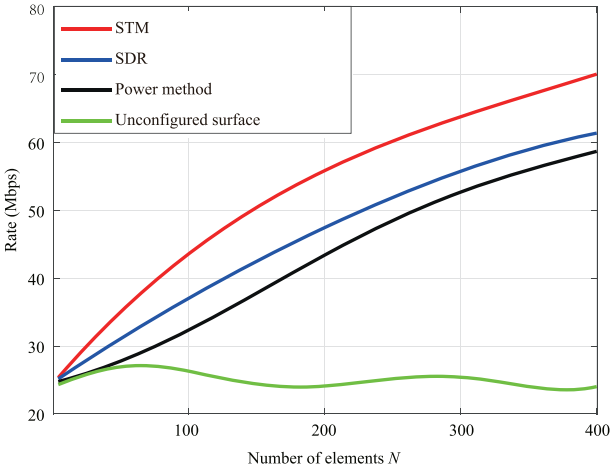

Fig. 5. Comparison of data rates for different values of *N*.

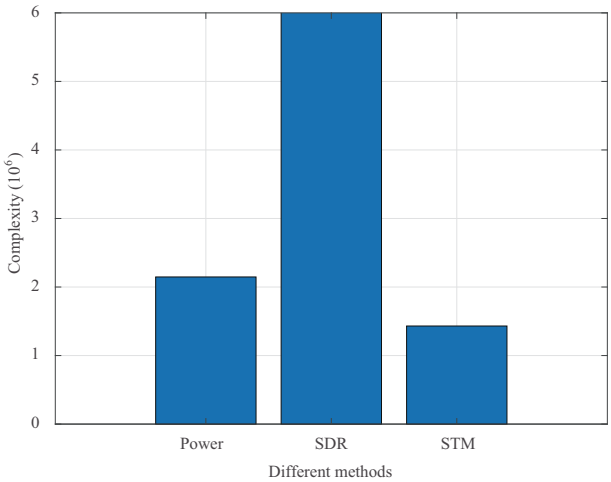

Fig. 6. Complexity level for each optimization method when $N = 400$.

complexity from $\mathcal{O}((N)+2(KM))$ to $\mathcal{O}((2N)+2(KM))$ due to assigning more phases for each RIS individual element and the switching between of them to aim the direction of the beamforming towards the receiver. Furthermore, the increase in the computational complexity $\mathcal{O}(2N)$ instead of $\mathcal{O}(N)$ is negligible and will increase the run time few seconds only. The challenge is clearly evident in the RIS hardware when higher-bit RIS is required. Generally speaking, it is required more PIN or varactor diodes for each RIS cell or element to achieve more states of phases so, it not recommended to complicate the design and increase the cost by selecting high-bit RIS while

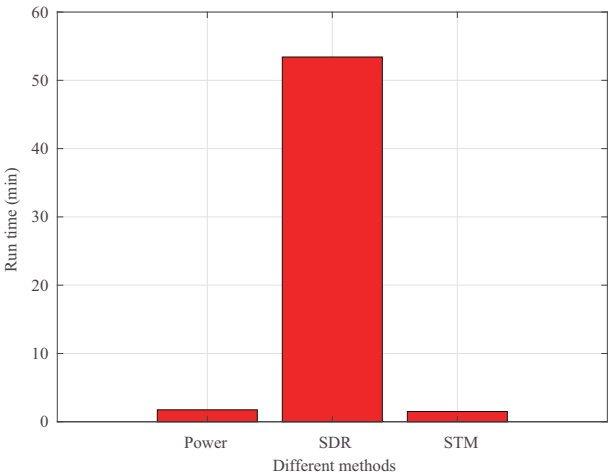

Fig. 7. Runtime consumption for each optimization method when $N = 400$.

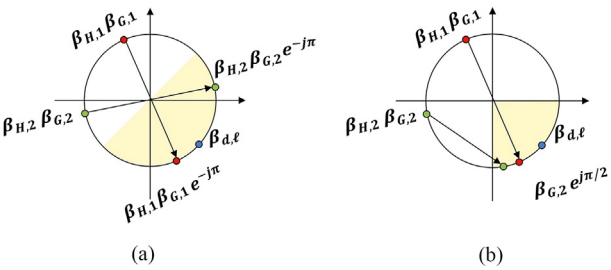

Fig. 8. (a). Two configurations: $\theta_n \in \{0, \pi\}$. (b). Four configurations: $\theta_n \in \{0, \pi, \pi/2, -\pi/2\}$.

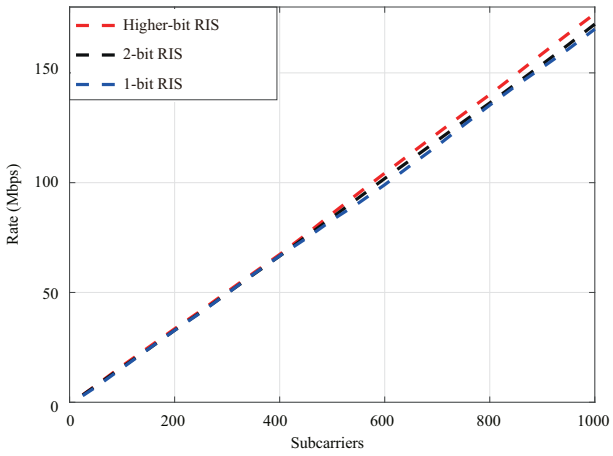

Fig. 9. STM method for multi-bit RIS design.

the 1-bit RIS phase profile can give comparable sum data rate performance. Fig. 9 shows the data rate for different bit RIS designs with slight difference in the performance for the STM scheme when $N = 900$ elements.

5. Conclusion

In this article, we showed that the RIS can be configured to provide significantly higher data rates, in comparison with a uniform surface, e.g., metal sheets. The codebook approach was implemented to generate varieties of phase configurations for the RIS surface in which we searched for the best configuration to be used in the optimization process. A problem formulation is described, and a solution is presented using different optimization methods and the water-filling algorithm. The data rate which is produced by different methods is compared with the upper bound. We noticed that all methods give performance near the upper bound, however, the data rate declines with the decrease in the dimensional area of the surface (number of elements per dimension). In addition, we have proved that the STM and the power methods are simple ways to configure the RIS with lower complexity and less runtime consumption. Selecting higher-bit RIS phase resolutions enhances slightly the sum data rate but at the cost of the hardware and computational complexities. The 1-bit RIS gives performance very close to the higher-bit phases which is enough to align the direct and the indirect paths constructively at the receiver. The RIS is a promising technology and is predicted to have a significant contribution in the 6G networks so, the search for low complex algorithms with reasonable data rate outcomes is crucial and necessary for realistic communications models.

Authors' contributions

S. Hassouna, M.A. Jamshed, Q.H. Abbasi: Conception and design of study, Simulation, Acquisition of data, Writing - original draft. Conception and design of study, Simulation, Acquisition of data. S. Hassouna, M.A. Jamshed, M. Ur-Rehman: Analysis and/or interpretation of data, Writing - original draft. M. Ur-Rehman, M.A. Imran: Writing - review and editing.

Declaration of competing interest

The authors declare that they have no known competing financial interests or personal relationships that could have appeared to influence the work reported in this paper.

References

[1] N.S. Perović, L.-N. Tran, M. Di Renzo, M.F. Flanagan, Achievable rate optimization for mimo systems with reconfigurable intelligent surfaces, IEEE Transactions on Wireless Communications 20 (6) (2021) 3865–3882.
[2] M. Di Renzo, A. Zappone, M. Debbah, M.-S. Alouini, C. Yuen, J. De Rosny, S. Tretyakov, Smart radio environments empowered by reconfigurable intelligent surfaces: How it works, state of research, and the road ahead, IEEE Journal on Selected Areas in Communications 38 (11) (2020) 2450–2525.
[3] E. Björnson, H. Wymeersch, B. Matthiesen, P. Popovski, L. Sanguinetti, E. de Carvalho, Reconfigurable intelligent surfaces: A signal processing perspective with wireless applications, IEEE Signal Processing Magazine 39 (2) (2022) 135–158.
[4] S. Hassouna, M.A. Jamshed, J. Rains, J.u.R. Kazim, M.U. Rehman, M. Abualhayja, L. Mohjazi, T.J. Cui, M.A. Imran, Q.H. Abbasi, A survey on reconfigurable intelligent surfaces: Wireless communication perspective, IET Communications 17 (5) (2023) 497–537.
[5] E. Björnson, Ö. Özdogan, E.G. Larsson, Intelligent reflecting surface versus decode-and-forward: How large surfaces are needed to beat relaying? IEEE Wireless Communications Letters 9 (2) (2020) 244–248.

[6] M. Di Renzo, K. Ntontin, J. Song, F.H. Danufane, X. Qian, F. Lazarakis, J. De Rosny, D.-T. Phan-Huy, O. Simeone, R. Zhang, M. Debbah, G. Lerosey, M. Fink, S. Tretyakov, S. Shamai, Reconfigurable intelligent surfaces vs. relaying: Differences, similarities, and performance comparison, IEEE Open Journal of the Communications Society 1 (2020) 798–807.
[7] C. Huang, A. Zappone, M. Debbah, C. Yuen, Achievable rate maximization by passive intelligent mirrors, in: Proceedings of the 2018 IEEE International Conference on Acoustics, Speech and Signal Processing (ICASSP), IEEE, 2018, pp. 3714–3718.
[8] H. Guo, Y.-C. Liang, J. Chen, E.G. Larsson, Weighted sum-rate maximization for intelligent reflecting surface enhanced wireless networks, in: Proceedings of the 2019 IEEE Global Communications Conference (GLOBECOM), IEEE, 2019, pp. 1–6.
[9] Y. Yang, B. Zheng, S. Zhang, R. Zhang, Intelligent reflecting surface meets ofdm: Protocol design and rate maximization, IEEE Transactions on Communications 68 (7) (2020) 4522–4535.
[10] E. Björnson, Optimizing a Binary Intelligent Reflecting Surface for Ofdm Communications under Mutual Coupling. https://doi.org/10.48550/arXiv.2106.04280.
[11] M.-M. Zhao, Q. Wu, M.-J. Zhao, R. Zhang, Intelligent reflecting surface enhanced wireless networks: Two-timescale beamforming optimization, IEEE Transactions on Wireless Communications 20 (1) (2021) 2–17.
[12] S. Zhang, R. Zhang, Capacity characterization for intelligent reflecting surface aided mimo communication, IEEE Journal on Selected Areas in Communications 38 (8) (2020) 1823–1838.
[13] S. Lin, B. Zheng, G.C. Alexandropoulos, M. Wen, F. Chen, S. sMumtaz, Adaptive transmission for reconfigurable intelligent surface-assisted ofdm wireless communications, IEEE Journal on Selected Areas in Communications 38 (11) (2020) 2653–2665.
[14] Q. Wu, R. Zhang, Intelligent reflecting surface enhanced wireless network via joint active and passive beamforming, IEEE Transactions on Wireless Communications 18 (11) (2019) 5394–5409.
[15] M. Cui, G. Zhang, R. Zhang, Secure wireless communication via intelligent reflecting surface, IEEE Wireless Communications Letters 8 (5) (2019) 1410–1414.
[16] Z. Chu, W. Hao, P. Xiao, J. Shi, Intelligent reflecting surface aided multi-antenna secure transmission, IEEE Wireless Communications Letters 9 (1) (2020) 108–112.
[17] P. Wang, J. Fang, X. Yuan, Z. Chen, H. Li, Intelligent reflecting surface-assisted millimeter wave communications: Joint active and passive precoding design, IEEE Transactions on Vehicular Technology 69 (12) (2020) 14960–14973.
[18] G. Yang, X. Xu, Y.-C. Liang, M. Di Renzo, Reconfigurable intelligent surface-assisted non-orthogonal multiple access, IEEE Transactions on Wireless Communications 20 (5) (2021) 3137–3151.
[19] G. Zhou, C. Pan, H. Ren, K. Wang, Z. Peng, Secure wireless communication in ris-aided miso system with hardware impairments, IEEE Wireless Communications Letters 10 (6) (2021) 1309–1313.
[20] M. Zeng, X. Li, G. Li, W. Hao, O.A. Dobre, Sum rate maximization for irs-assisted uplink noma, IEEE Communications Letters 25 (1) (2021) 234–238.
[21] B. Zheng, R. Zhang, Intelligent reflecting surface-enhanced ofdm: Channel estimation and reflection optimization, IEEE Wireless Communications Letters 9 (4) (2020) 518–522.
[22] P. Nuti, B.L. Evans, Spectral efficiency vs complexity in downlink algorithms for reconfigurable intelligent surfaces, in: Proceedings of the 2021 IEEE International Conference on Communications Workshops (ICC Workshops), IEEE, 2021, pp. 1–7.
[23] P. Nuti, E. Balti, B.L. Evans, Spectral Efficiency Optimization for Mmwave Wideband Mimo Ris-Assisted Communication. https://doi.org/10.48550/arXiv.2201.01739.
[24] S. Hassouna, J. Rains, J.R. Kazim, M.U. Rehman, M. Imran, Q.H. Abbasi, Discrete phase shifts for intelligent reflecting surfaces in ofdm communications, in: Proceedings of the 2022 International Workshop on Antenna Technology (iWAT), IEEE, 2022, pp. 128–131.
[25] X. Pei, H. Yin, L. Tan, L. Cao, Z. Li, K. Wang, K. Zhang, E. Björnson, Ris-aided wireless communications: Prototyping, adaptive beamforming, and indoor/outdoor field trials, IEEE Transactions on Communications 69 (12) (2021) 8627–8640.
[26] M. Grant, S. Boyd, Y. Ye, Cvx: Matlab Software for Disciplined Convex Programming, 2008.
[27] Spatial channel model for multiple input multiple output (mimo) simulations (release 6), https://portal.3gpp.org/desktopmodules/Specifications/SpecificationDetails.aspx?specificationId=1382.


Saber Hassouna

Saber Hassouna received the B.Sc. degree in electronics and telecommunication engineering from Misr University for science & technology, 6th october city, cairo, Egypt in 2004 and the M.Sc. from arab academy for science and technology and maritime transport Miami City, Alexanderia, Egypt, in 2007. He worked as a technical and design manager for low current, control and safety systems in UAE from 2009 until 2020. He is currently pursuing the Ph.D. degree with the Communications, Sensing, and Imaging (CSI) Group, James Watt School of Engineering, University of Glasgow, Glasgow, U.K., His research interests include wireless communication systems aided reconfigurable intelligent surfaces and near field localizations.


Muhammad Ali Jamshed

Muhammad Ali Jamshed earned a PhD degree in Electronics Engineering from the 5G/6G Innovation Centre, University of Surrey, UK, in 2021. He is endorsed by Royal Academy of Engineering under the exceptional talent category. He is a Fellow of Royal Society of Arts, and a Senior Member of IEEE. He was nominated for a Departmental Prize for Excellence in Research at the University of Surrey in 2019. Ali has contributed to three patents and authored/co-authored ten book chapters, edited one book and more than 50 technical articles in leading journals and at peer-reviewed conferences. He is also serving as an Associate Editor of IET Networks and founder of the workshop on Sustainable IoT for 6G and Beyond. Moreover, he served as a Reviewer, TPC, and Session Chair at many well-known conferences, such as ICC, WCNC, VTC, GlobeCom, and other scientific workshops.


Masood Ur Rehman

Masood Ur Rehman received the B.Sc. degree in electronics and telecommunication engineering from University of Engineering and Technology, Lahore, Pakistan in 2004 and the M.Sc. and Ph.D. degrees in electronic engineering from Queen Mary University of London, London, UK, in 2006 and 2010, respectively. He currently works as an Associate Professor at University of Glasgow. His research interests include compact antenna design, radiowave propagation, satellite navigation systems, electromagnetic wave interaction with human body, wireless sensor networks in healthcare and environmental monitoring and D2D/H2H communications. He has worked on several projects supported by industrial partners and research councils. He has contributed to a patent and authored/co-authored 5 books, 8 book chapters and more than 175 technical articles (with an h-index of 27) in leading journals and peer reviewed conferences. Dr. Ur-Rehman is a Fellow of the Higher Education Academy (UK), a member of the IET and BioEM and part of the technical program committees and organizing committees of several international conferences, workshops, and special sessions. He is a committee member of IEEE APS/SC WG P145, IEEE APS Best Paper Award committee and Pearson's focus group on formative assessment. He is acting as an associate editor of IEEE Sensors Journal, IEEE Access, IET Electronics Letters and Microwave & Optical Technology Letters, editorial advisor to CambridgeScholars Publishing, and lead guest editor of numerous special issues of renowned journals. He is vice-chair of IEEE APS/MTTS UKRI Chapter and acted as Workshop Chair for Workshop on Sustainable and Intelligent Green Internet of Things for 6G and Beyond in IEEE VTC-S 2022, TPC chair for UCET2020 and BodyNets2021 conferences.


Muhammad Ali Imran

Muhammad Ali Imran (a Fellow of IEEE) received the M.Sc. (Hons.) and Ph.D. degrees from Imperial College London, London, U.K., in 2002 and 2007, respectively. He is currently a Professor of Communication Systems with the University of Glasgow, U.K., and the Vice Dean with the Glasgow College UESTC. He is also an Affiliate Professor with The University of Oklahoma, USA, and a Visiting Professor with the University of Surrey, U.K. He is an Associate Editor for the IEEE Communications Letters, IEEE Access, and the IET Communications journal.


Qammer H. Abbasi

Qammer H. Abbasi is an academic with more than 12 years of research, leadership and teaching experience in prestigious institutes including Queen Mary University of London, University of Engineering and Technology Lahore, Texas A & M University at Qatar and University of Glasgow. He taught various courses both at undergraduate, graduate level and received teaching and research excellence awards. Dr. Abbasi has grant portfolio of £10 M and contributed to more than 500+ leading international technical journal (including Nature Communications, Nature Light: Science & Applications and Nature elight) and peer reviewed conference papers and 10 books and received several recognition for his research.